ACS Chemical Neuroscience

Research Article

pubs.acs.org/chemneuro

The Structures of the E22Δ Mutant-Type Amyloid-β Alloforms and the Impact of E22Δ Mutation on the Structures of the Wild-Type Amyloid-β Alloforms

Orkid Coskuner,*[,†,‡] Olivia Wise-Scira,[†] George Perry,[‡] and Taizo Kitahara[†]

[†]Department of Chemistry and [‡]Neurosciences Institute, The University of Texas at San Antonio, One UTSA Circle, San Antonio, Texas 78249, United States

Supporting Information

ABSTRACT: Structural differences between the intrinsically disordered fibrillogenic wild-type Aβ40 and Aβ42 peptides are linked to Alzheimer's disease. Recently, the E22Δ genetic missense mutation was detected in patients exhibiting Alzheimer's-disease type dementia. However, detailed knowledge about the E22Δ mutant-type Aβ40 and Aβ42 alloform structures as well as the differences from the wild-type Aβ40 and Aβ42 alloform structures is currently lacking. In this study, we present the structures of the E22Δ mutant-type Aβ40 and Aβ42 alloforms as well as the impact of E22Δ mutation on the wild-type Aβ40 and Aβ42 alloform structures. For this purpose, we performed extensive microsecond-time scale parallel tempering molecular dynamics simulations coupled with thermodynamic calculations. For studying the residual secondary structure component transition stabilities, we developed and applied a new theoretical strategy in our studies. We find that the E22Δ mutant-type Aβ40 might have a higher tendency toward aggregation due to more abundant β-sheet formation in the C-terminal region in comparison to the E22Δ mutant-type Aβ42 peptide. More abundant α-helix is formed in the mid-domain regions of the E22Δ mutant-type Aβ alloforms rather than in their wild-type forms. The turn structure at Ala21-Ala30 of the wild-type Aβ, which has been linked to the aggregation process, is less abundant upon E22Δ mutation of both Aβ alloforms. Intramolecular interactions between the N-terminal and central hydrophobic core (CHC), N- and C-terminal, and CHC and C-terminal regions are less abundant or disappear in the E22Δ mutant-type Aβ alloform structures. The thermodynamic trends indicate that the wild-type Aβ42 tends to aggregate more than the wild-type Aβ40 peptide, which is in agreement with experiments. However, this trend is vice versa for the E22Δ mutant-type alloforms. The structural properties of the E22Δ mutant-type Aβ40 and Aβ42 peptides reported herein may prove useful for the development of new drugs to block the formation of toxic E22Δ mutant-type oligomers by either stabilizing helical or destabilizing β-sheet structure in the C-terminal region of these two mutant alloforms.

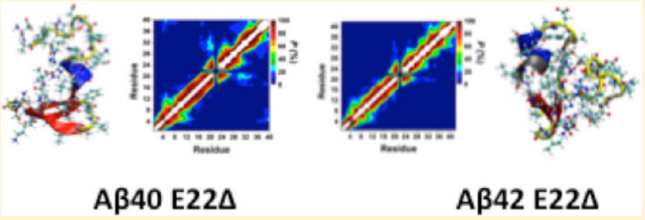

KEYWORDS: *Alzheimer's disease, amyloid-β, missense mutation, molecular dynamics simulations*

Proteolytic cleavage of the intrinsically disordered fibrillogenic amyloid-β precursor protein (APP) protein produces the 39−43 residue amyloid-β (Aβ) peptide, which is at the center of severe diseases including Alzheimer's disease.[1−3] Out of these Aβ alloforms, Aβ40 and Aβ42 have been identified as the most dominant and toxic fragments, respectively.[4−7] Genetically inherited forms of Alzheimer's disease are characterized by an early onset of Alzheimer's disease symptoms and can result from mutations of APP.[8,9] Several of the genetic missense mutations of APP are associated with familial Alzheimer's disease in which a single amino acid residue is affected in the sequence of Aβ.[10−13] Most recently, a genetic missense mutation that results in the deletion of the Glu22 residue (E22Δ, Osaka) of Aβ was reported in patients from a Japanese family exhibiting Alzheimer's-type dementia.[14] Even though the alloform specific differences in the toxicity for the wild-type Aβ40 and Aβ42 have recently been established,[5−7,15−20] these differences are debated in the current literature for the E22Δ mutant-type Aβ40 and Aβ42 alloforms.[14,21−24] Furthermore, the impact of the E22Δ mutation on the structures of the wild-type Aβ40 and Aβ42 peptides is poorly understood. For instance, Takuma et al. reported that wild-type Aβ42 is more toxic to mouse and human neuroblastoma cells than E22Δ mutant-type Aβ42 based on 3-(4,5-dimethylthiazo-2yl)-2,5-diphenyl tetrazolium bromide (MTT) assay measurements.[21] Ovchinnikova et al. showed similar findings using a lactate dehydrogenase (LDH) assay and have also proposed that Aβ40 neurotoxicity increases upon E22Δ mutation.[22] In contrast, Suzuki et al. reported that neither E22Δ mutant-type Aβ40 nor E22Δ mutant-type Aβ42 displays increased neurotoxicity for primary rat cortical neurons utilizing MTT and LDH assays in their experiments.[23] On the other hand, several experiments presented that the E22Δ mutation of

Received: September 6, 2012
Accepted: October 25, 2012
Published: October 25, 2012

Aβ inhibits the synaptic function of neurons.[14,21,23,24] Interestingly, Suzuki et al. proposed that the E22Δ mutant-type Aβ42 inhibits synaptic function more than the E22Δ mutant-type Aβ40 peptide.[23] Moreover, the E22Δ mutation was shown to promote oligomerization but not fibrillization of both Aβ alloforms based on thioflavin T (ThT) fluorescence and Western blotting experiments as well as Pittsburgh compound B positron emission topography scans of affected patients.[14] On the other hand, several other studies have reported that the E22Δ mutation significantly enhances the rate of fibrillization of Aβ based on ThT fluorescence and electron microscopy measurements.[22,23,25−27] Poduslo et al. reported that E22Δ mutant-type Aβ40 forms fibrils faster than E22Δ mutant-type Aβ42 based on time dependent electron microscopy measurements.[26] Despite this, ThT fluorescence and electron microscopy experiments by other groups presented that E22Δ mutant-type Aβ42 aggregates more rapidly than E22Δ mutant-type Aβ40.[22,23,25] In addition, various electron microscopy studies reported different structures for the E22Δ mutant-type Aβ fibrils. For example, Inayathullah and Teplow reported unbranched fibril structures for both the wild-type and E22Δ mutant-type Aβ alloforms with a few twisted or curved E22Δ mutant-type Aβ40 fibrils.[25] However, Ovchinnikova et al. proposed that E22Δ mutant-type Aβ40 forms fibrillar bundles instead of distinct fibrils whereas the wild-type Aβ40 forms straight fibrils with some small bundles present and the wild- and E22Δ mutant-type Aβ42 peptides adopt discrete twisted fibrils.[22] Parallel to these findings, Meredith and co-workers presented large fibrillar bundle formations of the E22Δ mutant-type Aβ40 structures.[27]

Experiments using conventional tools face numerous challenges associated with rapid conformational changes, fast aggregation kinetics, and solvent effects. These challenges might be a reason for the existing debate about the toxicity and structural properties of the E22Δ mutant-type Aβ40 and Aβ42 peptides in the current literature. Theoretical studies can complement experiments by providing molecular level knowledge. Recently, we reported with Murray and co-workers the structural and thermodynamic differences between the wild-type, methionine oxidized, and E22Δ mutant-type Aβ42 peptides that occur in the presence and absence of sodium dodecyl sulfate (SDS).[28] To the best of our knowledge, a study that investigates the structural properties of the monomeric E22Δ mutant-type Aβ40 and Aβ42 peptides, and compares these properties to those of the full-length wild-type Aβ40 and Aβ42 in an aqueous solution environment has not yet been performed. In this study, we present the dynamic changes in the structural and thermodynamic properties of the E22Δ mutant-type Aβ40 and Aβ42 alloforms in an aqueous solution. Moreover, we present the impact of E22Δ mutation on the structures of the wild-type Aβ40 and Aβ42 alloforms in an aqueous solution environment. Furthermore, we also apply a new method that we developed, which enables the determination of secondary structure component conversions at the atomic level with dynamics. For these purposes, we performed extensive parallel tempering molecular dynamics simulations coupled with thermodynamic calculations. The changes in the enthalpic and entropic contributions to the conformational Gibbs free energies are provided for the E22Δ mutant-type as well as the wild-type Aβ40 and Aβ42 alloforms, and these properties are compared to one another. The secondary and tertiary structural properties of the E22Δ mutant-type Aβ40 and Aβ42 are determined and compared to those calculated for the wild-type Aβ40 and Aβ42 peptides. Given that the formation of specific secondary structures, such as β-sheet, are directly linked to the aggregation mechanism and toxicity of Aβ, the secondary structure transition stabilities become a crucial component in these investigations.[18,29−31] For gaining more detailed insights into the dynamic secondary structure properties of proteins, we apply a new theoretical strategy that we developed to calculate the transition stabilities between two different residual secondary structure components. This method provides an understanding of the residual secondary structure conversion stabilities in the structures of the wild- and E22Δ mutant-type Aβ40 and Aβ42 alloforms. Our results clearly demonstrate that the E22Δ mutation impacts the structural and thermodynamic properties of the wild-type Aβ40 and Aβ42 peptides at the monomeric level in an aqueous solution environment.

RESULTS AND DISCUSSION

The secondary structure formations, such as α-helix and β-sheet, are crucial in the studies of intrinsically disordered fibrillogenic protein structures at the center of neurodegenerative diseases due to their roles in the aggregation processes and toxicity.[18,29−31] We investigated the secondary structure properties using a widely utilized software package, DSSP,[32] as well as our own new code implemented in our ProtMet software package that allows the determination of the secondary structure transition stabilities (see Methods and Supporting Information). Based on our calculations, the most abundant residual secondary structures are the coil and turn conformations in all wild- and mutant-type peptides (Figure 1). The average overall abundances of α-helix in the N-terminal region (Asp1-Lys16) of the wild-type Aβ40 and Aβ42 and the E22Δ mutant-type Aβ42 peptides are similar (17% and 19%). However, the overall α-helical structure abundance is larger (30%) in the same region of the E22Δ mutant-type Aβ40, indicating that E22Δ mutation increases α-helix prominence in the N-terminal region of Aβ40 (Figure 1A). Specifically, Arg5-Asp7 and Tyr10-Lys16 in Aβ40 show an increase upon E22Δ mutation (up to 36%). Using specific residual analysis, we detect that Phe4-Asp7 of Aβ42 adopts less abundant α-helix (≤19%) upon E22Δ mutation while an increase in α-helix prominence (up to 21%) is observed for Ser8-Lys16 (Figure 1B). The overall β-sheet contents in the N-terminal regions of the wild- and E22Δ mutant-type Aβ42 are small (0.4−0.9%). The wild-type Aβ40 presents slightly larger overall β-sheet content in the N-terminal region (2.3%) which disappears upon E22Δ mutation (Figure 1A), indicating that the oligomerization and fibrillization process involving the β-sheet forming residues located in the N-terminal region of Aβ40 is less likely in the E22Δ mutant-type Aβ40 peptide in comparison to its wild-type form (Figure 1A). Regarding the formation of the turn structure differences, the largest discrepancies occur at His14-Lys16 of Aβ40 (with a decrease up to 29%) and at Arg5-Val12 of Aβ42 (with a decrease up to 35%) upon E22Δ mutation (Figure 1B).

The overall α-helix abundance is 9.5% and 12.7% larger in the mid-domain region (Leu17-Ala30) of the E22Δ mutant-type Aβ40 and Aβ42 in comparison to the wild-type Aβ40 and Aβ42, respectively (Figure 1). Specifically, Leu17-Phe19, Ala21, and Asp23-Lys28 adopt more prominent α-helix (up to 9%) in the structures of E22Δ mutant-type Aβ40 in comparison to the wild-type Aβ40 peptide (Figure 1A). The same residues and additionally Phe20 form more prominent α-helix (up to 28%)

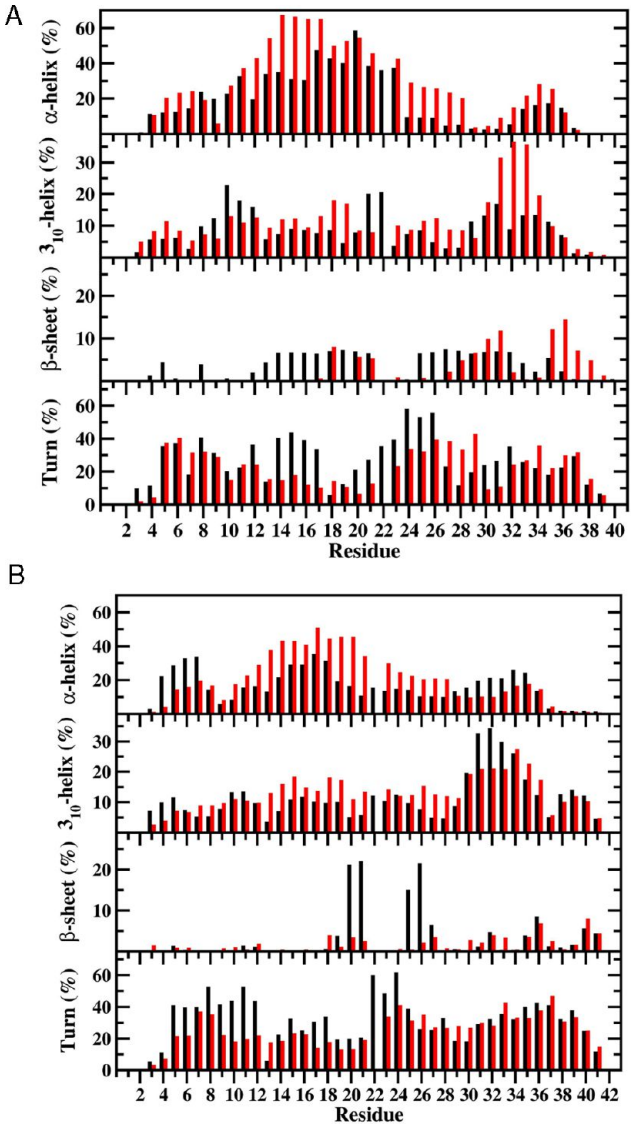

Figure 1. Calculated secondary structure abundances per residue for the (a) wild-type (black) and E22Δ mutant-type (red) Aβ40 and (b) wild-type (black) and E22Δ mutant-type (red) Aβ42 peptides in aqueous solution. The abundances for the π-helix and coil structures are not displayed.

in the structures of Aβ42 upon E22Δ mutation (Figure 1B). The same region presents a slight decrease of β-sheet prominence in the structures of the E22Δ mutant-type Aβ40 (2.0%) and Aβ42 (4.9%) in comparison to their wild-type forms (Figure 1). Namely, Leu17, Phe19-Ala21, and Gly25-Lys28 adopt less prominent β-sheet in the structures of Aβ40 and Aβ42 upon E22Δ mutation. Interestingly, the overall turn structure abundance decreases by 6.4% and 7.3% in the structures of E22Δ mutant-type Aβ40 and Aβ42 in comparison to the wild-type Aβ40 and Aβ42 peptides, respectively. The turn structure formation in the Ala21-Ala30 region has been related to the distinct structuring of the disordered protein as well as to its aggregation mechanism and toxicity.[15,19,33−39] We find that Ala21-Ser26 and Ala30 of E22Δ mutant-type Aβ40 and Ala21-Gly25 and Lys28 of E22Δ mutant-type Aβ42 adopt less abundant turn structure by 12−34% and up to 58% in comparison to their wild-type forms, respectively. These results might indicate that Ala21-Ala30 is less reactive toward aggregation in the structures of the E22Δ mutant-type Aβ40 and Aβ42 peptides in comparison to the same region in the wild-type Aβ40 and Aβ42 peptides. We should mention here that β-sheet formation in the central hydrophobic core (CHC; Leu17-Ala21) region decreases its abundance up to 7% and 18% in the structures of Aβ40 and Aβ42 upon E22Δ mutation, respectively. This finding indicates that the reactivity of the CHC region toward aggregation is depressed in E22Δ mutant-type in comparison to the wild-type Aβ alloforms.

For the C-terminal region, we note an interesting trend in the helix structures; Ile31-Met35 adopt more abundant α-helix in the structures of the E22Δ mutant-type Aβ40 in comparison to the same region in its wild-type form, while the opposite trend is detected for the same residues of the E22Δ mutant-type and wild-type Aβ42 peptides (Figure 1B). Furthermore, 3$_{10}$-helix formation increases sharply for Ile31-Leu34 in the structures of the E22Δ mutant-type Aβ40 peptide in comparison to its wild-type form (Figure 1A). On the other hand, 3$_{10}$-helix formation is decreased by 11−14% at Ile31-Gly33 in Aβ42 upon E22Δ mutation (Figure 1B). The β-sheet formation in the C-terminal region of the E22Δ mutant-type Aβ42 does not differ significantly from that of the wild-type Aβ42 that we reported most recently.[40] However, Ile31, Met35-Val39 adopt more abundant β-sheet (up to 12%) in the structures of the E22Δ mutant-type Aβ40 peptide in comparison to its wild-type form (Figure 1A). This result indicates an increased tendency toward aggregation via the C-terminal region of the E22Δ mutant-type Aβ40 in comparison to the wild-type Aβ40 peptide. Overall, the calculated secondary structure properties for the wild-type alloforms, for which experimental and theoretical data exist, are in excellent agreement with previously performed studies.[15−18,40,41]

Figure 2 presents the free energy values for secondary structure transitions between two different secondary structure components per residue based on our free energy calculation method (see the Methods and Supporting Information for further details). Using these figures, we can identify which secondary structure component is most likely to result in the formation of a specific secondary structure of interest. For example, the secondary structure component before the formation of β-sheet structure provides insights into the nature of dynamic β-sheet structure formation pathway, which is currently in accessible using conventional experimental tools. Based on these free energy calculations, the most favorable secondary structure component transition occurs for turn or helix to coil and turn to helix in the structures of the wild-type Aβ40 peptide (Figure 2, Aβ40). Regarding the helix formation in the N-terminal region of Aβ40, turn to helix transition is most preferred at Glu3-Lys16. We also detect that Phe4, Arg5, Ser8, and Val12 in the N-terminal region of the wild-type Aβ40 present more stable coil to β-sheet conversion rather than other possible secondary structure transitions resulting in β-sheet formation. In addition, turn or helix to β-sheet conversions are thermodynamically preferred at His13-Lys16 of Aβ40. Interestingly, transitions resulting in the formation of β-sheet structure in the N-terminal region are less preferred for the E22Δ mutant-type Aβ40 in comparison to its wild-type form (Figure 2, Aβ40 E22Δ). Furthermore, residues Asn27, Lys28, Met35, and Val36 possess more stable helix to β-sheet structure conversion while the opposite trend is observed in the CHC region upon E22Δ mutation of Aβ40. Gly25 and Ser26 adopt less favorable β-sheet to turn structure transition in the E22Δ mutant-type Aβ40 rather than in the wild-type Aβ40 peptide. In

dx.doi.org/10.1021/cn300149j | ACS Chem. Neurosci. 2013, 4, 310−320

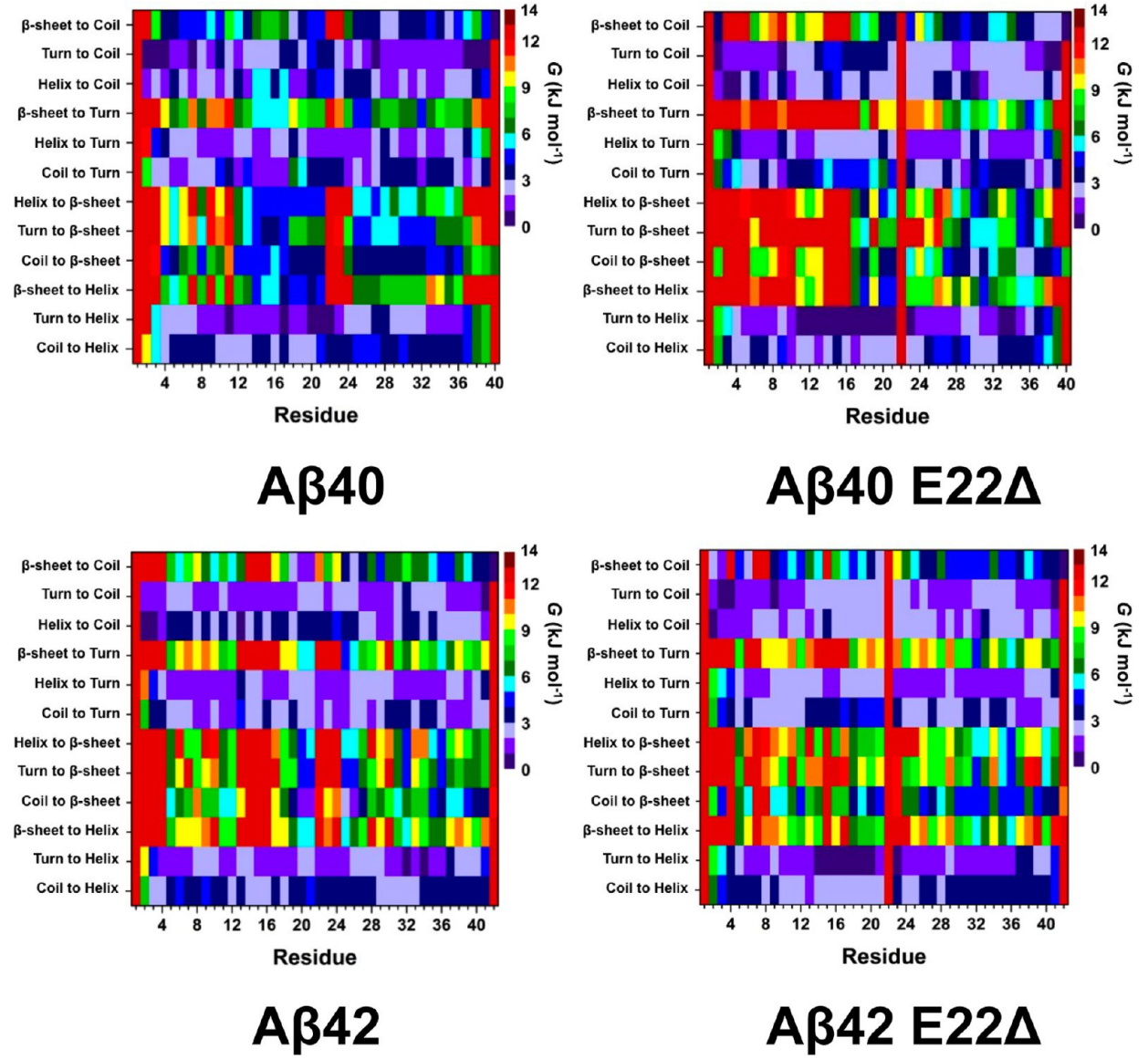

Figure 2. Stability of secondary structure transitions between two specific secondary structure components per residue for the wild-type Aβ40 (Aβ40), E22Δ mutant-type Aβ40 (Aβ40 E22Δ), wild-type Aβ42 (Aβ42), and E22Δ mutant-type Aβ42 (Aβ42 E22Δ) peptides in aqueous solution. The color scale corresponds to the free energy value associated with specific transitions between two secondary structure components for a specific residue.

comparison to wild-type Aβ40, the wild-type Aβ42 peptide possesses less preferred β-sheet to helix transition in the CHC region (Figure 2, Aβ42). Furthermore, parts of the N- and C-terminal and mid-domain regions of Aβ42 present less stable coil to β-sheet transitions relative to Aβ40. Instead, Met35-Ala42 converts from coil to β-sheet more favorably in the structures of Aβ42 than in Aβ40 (Figure 2). Residues Ile32 and Val36 present preferred turn or helix to β-sheet transition in the structures of the wild-type Aβ42 peptide. Differences in the secondary structure transition stabilities occur between Aβ40 and Aβ42 for conversions resulting in turn structure formation. For instance, β-sheet or helix to turn transitions in the protease resistant region are more preferred in Aβ42 rather than in Aβ40. Both helix to β-sheet and β-sheet to helix are more favorable at His14-Ala21 for Aβ40 in comparison to the same region of Aβ42. In comparison to the wild-type Aβ42, more stable coil to β-sheet conversion exists at Glu3, Val12, and Ala30-Ile32 and less preferred coil or helix to β-sheet transition occurs at Phe19-Ala21, Gly25, and Ser26 in the structures of the E22Δ mutant-type Aβ42 monomer (Figure 2, Aβ42 E22Δ). Furthermore, coil to turn conversion in parts of the N-terminal and CHC regions becomes slightly less favorable upon E22Δ mutation of Aβ42.

Figure 3 depicts the probability of intramolecular interactions occurring between any two residues of the Aβ protein. Interactions along the main diagonal in these figures correspond to the residues that are located adjacent to each other within the Aβ sequence and thus are expected to be in contact for all wild-type and E22Δ mutant-type Aβ structures. However, those intramolecular interactions that occur off of the main diagonal represent interactions between amino acid residues that are non-adjacent and therefore are associated with the overall tertiary structure of the wild- and E22Δ mutant-type alloforms. Based on these figures, the tertiary structures of the wild-type alloforms differ from those calculated for the monomeric E22Δ mutant-type alloforms

dx.doi.org/10.1021/cn300149j | ACS Chem. Neurosci. 2013, 4, 310−320

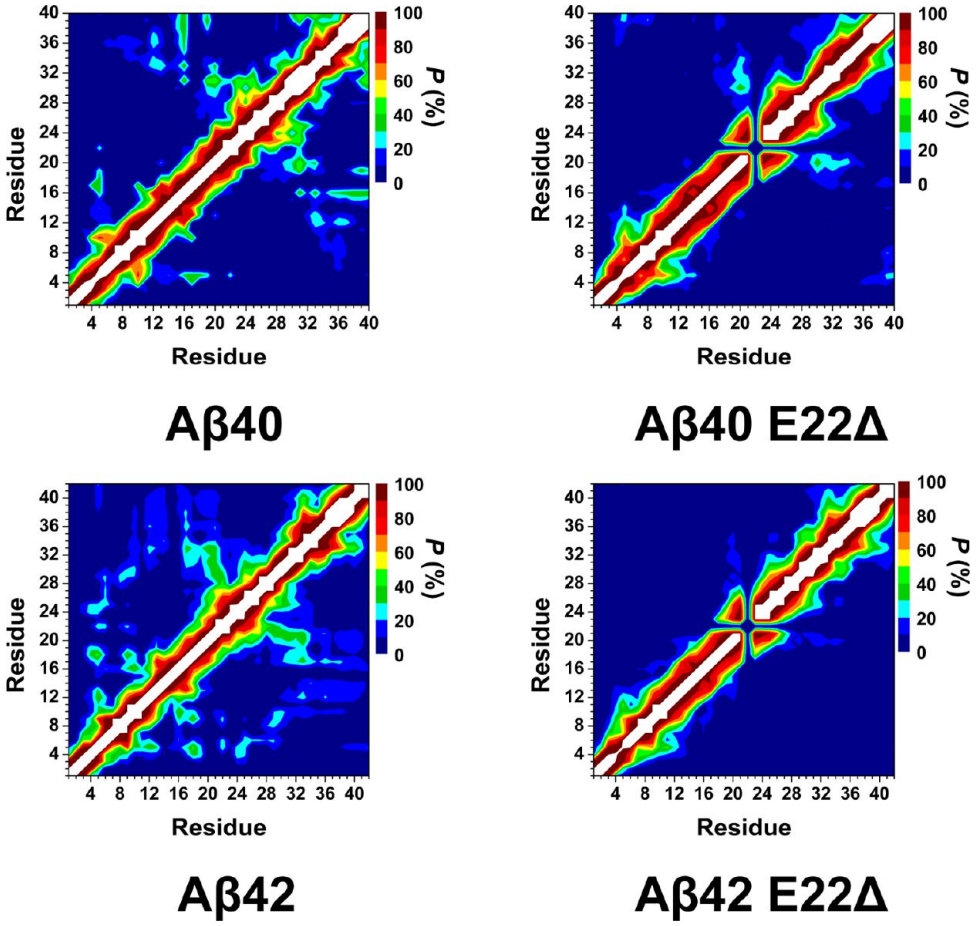

Figure 3. Calculated intramolecular interactions of the wild-type Aβ40 (Aβ40), E22Δ mutant-type Aβ40 (Aβ40 E22Δ), wild-type Aβ42 (Aβ42), and E22Δ mutant-type Aβ42 (Aβ42 E22Δ). The color scale corresponds to the probability (P) of the distance between the centers of mass between two residues being ≤9 Å from each other.

(Figure 3). A comparison between the wild- and E22Δ mutant-type Aβ40 monomers shows significant differences within the N-terminal, mid-domain, and C-terminal regions. Furthermore, we note that various interactions, such as those between the N-terminal and CHC region, the N- and C-terminal regions, and CHC region and C-terminal regions, either become less abundant or disappear upon E22Δ mutation of Aβ40. Interestingly, the same trend is observed for the interactions between the N-terminal and CHC regions, N- and C-terminal regions, mid-domain, and C-terminal regions of the wild-type Aβ42 peptide in comparison to the E22Δ mutant-type Aβ42 peptide. Additionally, Phe4-His6 interacts less abundantly with Val12-His14 in the E22Δ mutant-type Aβ42 than in the E22Δ mutant-type Aβ40 peptide structures. However, the vice versa trend is obtained for interactions between Leu17-Ala21 and Ala30-Leu34 in the E22Δ mutant-type Aβ alloforms. The N- and C-terminal regions (Phe4-Gly9 with Val36-Val40) interact in the structures of the E22Δ mutant-type Aβ40 peptide but not in the E22Δ mutant-type Aβ42 peptide structures. Overall, these findings suggest that the E22Δ mutant-type Aβ alloforms possess less compact structures in comparison to their wild-type forms in aqueous solution. Furthermore, the E22Δ mutant-type Aβ42 structures are slightly less compact than those of the E22Δ mutant-type Aβ40 peptide. The calculated tertiary structures for the wild-type Aβ alloforms are in excellent agreement with previous theoretical and experimental studies.[15,17−19,42,43]

We reported recently that Arg5 forms stable salt bridges with various residues located in the N-terminal, mid-domain, and C-terminal regions of the wild-type Aβ42 peptide.[40] This study shows that Arg5 also forms prominent salt bridges with Asp1, Glu11, Glu22, and Val40 in the structures of the wild-type Aβ40 peptide (Table 1). Interestingly, the salt bridges formed by Arg5 with Asp1, Glu11, Glu22, or Val40 decrease by 5−18% for the E22Δ mutant-type Aβ40 in comparison to the wild-type Aβ40. Moreover, salt bridge abundances between Lys16 and Glu3, Asp7, Glu11, Glu22, or Val40 decrease up to 30% upon E22Δ mutation of Aβ40. Similarly, the abundance of the salt bridges formed between Arg5 and Asp1, Asp23, or Ala42 is smaller in the E22Δ mutant-type Aβ42 structures in comparison to those of the wild-type Aβ42 peptide. The salt bridge between Asp23 and Lys28 is slightly more stable in the structures of Aβ40 rather than those of Aβ42, which is in agreement with previous studies.[15,17,43] Interestingly, this trend is inversed for the E22Δ mutant-type alloforms. We also calculated the salt bridge stability distribution between Asp23 and Lys28 (Figure 4) via comparing the distributions of the distances between the C^{γ} (Asp23) and N^{ζ} (Lys28) atoms. At a distance of 4.0 Å between the C^{γ} and N^{ζ} atoms, the Asp23 and Lys28 salt bridge is more stable in the E22Δ mutant-type alloforms in comparison to their wild type forms. However, the salt bridge between Asp23 and Lys28 is more stable in the E22Δ mutant-type Aβ42 than the E22Δ mutant-type Aβ40 peptide.

dx.doi.org/10.1021/cn300149j | ACS Chem. Neurosci. 2013, 4, 310−320

Table 1. Formed Salt Bridges of the Wild-Type and E22Δ Mutant-Type Aβ40 and Aβ42 Peptides[a]

		$R(C^{\gamma}-N^{\zeta}) \leq 4$ Å (%)			
donor	acceptor	Aβ40	Aβ40 ΔE22	Aβ42	Aβ42 ΔE22
Arg5	Glu3	100.0	100.0	100.0	100.0
Arg5	Glu22	70.1		10.3	
Arg5	Asp1	43.9	26.3	31.2	19.1
Lys16	Val40/Ala42 ($-COO^-$)	36.8	5.3	2.2	0.8
Arg5	Glu11	32.9	68.5	65.5	39.0
Arg5	Val40/Ala42 ($-COO^-$)	30.3	60.8	31.8	20.6
Lys16	Glu11	17.3	4.2	2.4	2.6
Lys28	Glu22	11.4	-	3.1	-
Lys28	Val40/Ala42 ($-COO^-$)	6.5	0.9	3.4	2.9
Lys28	Asp23	4.0	6.8	1.6	8.1
Lys16	Glu22	3.8	-	4.5	-
Arg5	Asp7	1.7	3.6	0.2	7.4
Lys16	Asp7	0.1	10.5	0.8	6.2
Lys16	Glu3	0.0	3.0	0.0	0.2
Asp1 ($-NH_3^+$)	Glu3	0.6	2.0	0.1	0.6
Arg5	Asp23	0.0	0.5	27.9	0.7
Lys28	Glu11	0.0	0.0	0.0	1.8
Lys16	Asp23	0.1	0.1	1.4	0.2

[a] $R(C^{\gamma}-N^{\zeta})$ is the distance between carboxylate C atom (C^{γ}) and the side-chain or N-terminus N atom (N^{ζ}).

The calculated conformational Gibbs free energies using harmonic and quasi-harmonic methods are listed along with the enthalpy and entropy values in Table 2. The same trends are observed using either a harmonic or a quasi-harmonic method in our simulations. Namely, the structures of the wild-type Aβ42 are less stable than those of the wild-type Aβ40 peptide in an aqueous solution environment. These conformational Gibbs free energies support previous studies that reported a higher tendency toward aggregation for the wild-type Aβ42 rather than the wild-type Aβ40.[44−47] Both E22Δ mutant-type alloforms are less stable than their wild-type forms but the trend between the two different alloforms is inversed upon E22Δ mutation. Specifically, the E22Δ mutant-type Aβ42 structures are more stable than those of the E22Δ mutant-type Aβ40. Based on these findings, the E22Δ mutant-type Aβ40 has a slightly larger tendency toward aggregation in comparison to the E22Δ mutant-type Aβ42 peptide in an aqueous solution environment. When we analyze these thermodynamic results along with the structural properties that we report above, we obtain interesting insights into the structure and function relationships of the wild- and mutant-type Aβ peptides. The free energy landscapes of all wild-type and mutant-type peptides based on their end-to-end ($R_{E\text{-}E}$) distance and radius of gyration (R_g) distributions were calculated (Figure 5). These free energy landscapes identify the conformational preferences of the wild-type and E22Δ mutant-type Aβ40 and Aβ42 structures in aqueous solution based on their R_g and $R_{E\text{-}E}$ values. The most favorable or most preferred structures occur in the regions with the lowest change in potential of mean force (PMF) values. These preferred structures are localized to specific regions, which are termed basins. As described in one of our recent studies of the wild-type Aβ42 peptide,[40] there are two most preferred PMF basins (Figure 5, Aβ42; basins IA and IB) and transitions between basins IA and IB require overriding

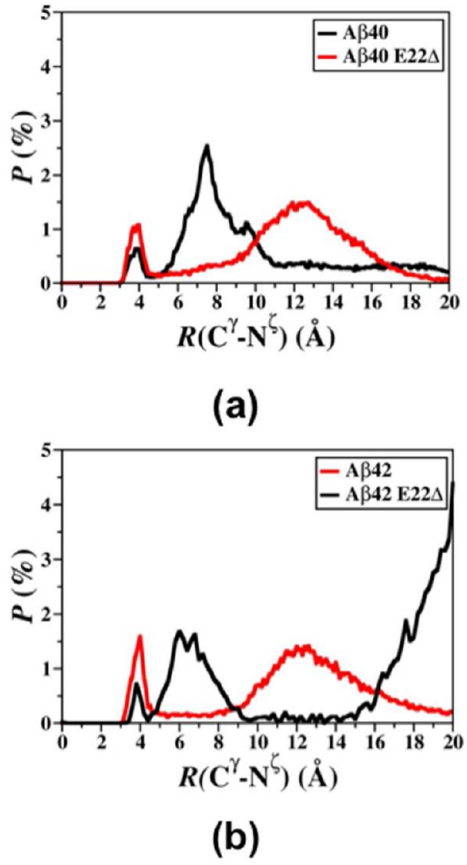

Figure 4. Calculated probability distribution of the distance between the C^{γ} atom of the Asp23 residue and the N^{ζ} atom of the Lys28 residue for all converged structures of the (a) Aβ40 and (b) Aβ42 wild-type (black) and E22Δ mutant-type (red) peptides.

of large energy barriers that are larger than 1 k_BT. We find a similar trend for the wild-type Aβ40 peptide. Specifically, the most preferred basins are located at R_g values varying between 9 and 11.4 Å (basin IA) and 9.1 and 13.2 Å (basin IB) with corresponding $R_{E\text{-}E}$ values of 9.9−17.5 Å (basin IA) and 17.6 −34.8 Å (basin IB) for Aβ40 (Figure 5, Aβ40). For the E22Δ mutant-type Aβ42 peptide, we detect only one most favorable basin (Figure 5, Aβ42 E22Δ; R_g = 10−11 Å; $R_{E\text{-}E}$ = 12.7−16.9 Å). However, E22Δ mutant-type Aβ40 adopts two most preferred basins with similar PMF values basin IA (Figure 5, Aβ40 E22Δ; R_g = 10.2−10.8 Å; $R_{E\text{-}E}$ = 10.0−17.0 Å) and basin IB (R_g = 9.8−11.8 Å; $R_{E\text{-}E}$ = 17.5−22.0 Å), but transitioning between basins IA to IB or vice versa does not require overriding large energy barriers (<1 k_BT). The secondary and tertiary structure properties belonging to these specific basins are analyzed to understand the trends along the free energy surface and are presented in the Supporting Information.

Overall, the conformational Gibbs free energies using harmonic and quasi-harmonic methods show that the aqueous E22Δ mutant-type Aβ40 structures are slightly less stable than the aqueous E22Δ mutant-type Aβ42 conformations. Our findings support experiments that proposed a higher tendency toward aggregation for E22Δ mutant-type Aβ40 rather than for the E22Δ mutant-type Aβ42 peptide.[26] The structural properties of the wild- and E22Δ mutant-type alloforms differ starkly from each other. For instance, the α-helix content in the N-terminal region of E22Δ mutant-type Aβ40 is larger than that of the other three peptides. In comparison to the wild-type

dx.doi.org/10.1021/cn300149j | ACS Chem. Neurosci. 2013, 4, 310−320

Table 2. Calculated Mean Values of Potential Energy (E), Solvation Free Energy ($G_{sol.}$), Enthalpy (H), Entropy (TS), and Gibbs Free Energy (G) for the Wild-Type and $\Delta E22$ Mutant-Type Aβ40 and Aβ42 Peptides Using the Normal Mode Analysis (S_{NMA}) and Schlitter (S_{QM}) Methods to Calculate the Entropic Contribution to G

	$\langle E_{total}\rangle$	$\langle G_{sol}\rangle$	$\langle H\rangle$	$-T\langle S_{NMA}\rangle$	$-T\langle S_{QH}\rangle$	$\langle G_{NMA}\rangle$	$\langle G_{QH}\rangle$
Aβ40	−780.5 (±180.2)	−2007.7 (±125.9)	−2788.2 (±55.6)	−2114.4 (±9.9)	−5334.3 (±78.2)	−4902.5 (±45.9)	−8361.5 (±95.9)
Aβ42	−175.4 (±44.6)	−2404.5 (±27.3)	−2579.9 (±24.2)	−2206.6 (±4.1)	−5781.3 (±131.3)	−4786.5 (±20.3)	−8122.2 (±93.5)
E22Δ Aβ40	−203.7 (±93.7)	−1999.0 (±71.5)	−2202.7 (±41.0)	−2177.7 (±10.5)	−5810.1 (±123.3)	−4380.4 (±30.7)	−7821.8 (±99.9)
E22Δ Aβ42	−598.1 (±112.7)	−1856.9 (±76.3)	−2454.9 (±38.3)	−2072.9 (±8.7)	−5367.0 (±86.6)	−4526.6 (±30.5)	−8012.7 (±94.7)

Aβ40 peptide, the β-sheet content disappears in the N-terminal region of the E22Δ mutant-type Aβ40 peptide. Interestingly, more abundant α-helix is formed while the β-sheet prominence decreases in the mid-domain regions of the E22Δ mutant-type Aβ40 and Aβ42 peptides rather than in the same region of their wild-type forms. The turn structure formation in the Ala21-Ala30 region of the wild-type Aβ peptide, which is linked to the aggregation process, is less abundant in the structures of the E22Δ mutant-type Aβ40 and Aβ42 peptides in an aqueous solution environment. On the other hand, α-helix and 3_{10}-helix abundances are larger in the C-terminal regions of the E22Δ mutant-type Aβ40 and Aβ42 peptides rather than the wild-type peptides. No stark differences are detected for the adopted β-sheet abundances in the C-terminal regions upon E22Δ mutation of Aβ42. β-Sheet content is larger at Ile31 and Met35-Val39 in the C-terminal region of the E22Δ mutant-type Aβ40 rather than in the same region of the wild-type Aβ42 peptide.

The thermodynamic stabilities of secondary structure component transitions at the atomic level with dynamics have been addressed for the first time in this work. We find that β-sheet to turn or helix transitions are more favorable at Ala21-Ala30 of the wild-type Aβ42 in comparison to the wild-type Aβ40 peptide. Both the helix to β-sheet and β-sheet to helix transitions are more preferred at His14-Ala21 in the structures of the wild-type Aβ40 in comparison to those in the conformations of the wild-type Aβ42. The coil to β-sheet as well as helix to β-sheet conversions are less favorable at Phe19-Ala21, Gly25, and Ser26 in the structures of the E22Δ mutant-type Aβ42 rather than those of the wild-type Aβ42 peptide. Moreover, less preferred coil to turn transitions exist in the N-terminal and CHC regions of the E22Δ mutant-type Aβ42 rather than in the structures of the wild-type Aβ42 peptide. Stark differences in the tertiary structure properties occur between the E22Δ mutant-type A40 and Aβ42 peptides and their wild-type forms. For instance, intramolecular interactions between the N-terminal and CHC, N-and C-terminal, or CHC and C-terminal regions that occur in the wild-type Aβ alloforms are either less abundant or disappear in the structures of the E22Δ mutant-type Aβ40 and Aβ42 alloforms. In addition, we detect less abundant intramolecular interactions between the C-terminal and mid-domain regions in the upon E22Δ mutation of structures of Aβ42 in an aqueous solution environment. Moreover, salt bridge stabilities are lower in the structures of the E22Δ mutant-type Aβ40 and Aβ42 rather than those of the wild-type Aβ alloforms. The stability of the salt bridge between the residues Asp23 and Lys28 has been directly related to the turn structure formation in the Ala21-Ala30 region of the wild-type Aβ peptide,[15,17,43,48] and we detect that the stability of this salt bridge is larger in the structures of the wild-type Aβ40 in comparison to the wild-type Aβ42. Interestingly, this trend is vice versa in the structures of the E22Δ mutant-type Aβ40 and Aβ42 alloforms. Additionally, we find that the free energy landscapes of the E22Δ mutant-type Aβ40 and Aβ42 peptides based on their radius of gyration and end-to-end distances differ from those calculated for the wild-type Aβ40 and Aβ42 alloforms.

In agreement with previous experimental and theoretical studies,[15,17−19,43] we detect that the β-sheet abundance in the C-terminal region of the wild-type Aβ42 is larger than that in the structures of the wild-type Aβ40 peptide. Surprisingly, we find that this trend is different in the structures of the E22Δ mutant-type Aβ40 and Aβ42 alloforms; the β-sheet abundance is larger in the C-terminal region of the E22Δ mutant-type Aβ40 rather than in its wild-type form. However, we cannot detect a significant difference between the β-sheet abundances in the C-terminal regions of the wild- and E22Δ mutant-type Aβ42 peptides. In other words, these findings indicate that the tendency toward oligomerization, fibrillization and aggregation might be larger for the E22Δ mutant-type Aβ40 peptide in comparison to its wild-type form via the participation of β-sheet forming residues in the C-terminal region. On the other hand, such a difference for the wild- and E22Δ mutant-type Aβ42 peptides could not be detected. Furthermore, our studies show that the structures of the wild-type Aβ40 and Aβ42 are more compact in an aqueous solution environment in comparison to the conformations of the E22Δ mutant-type Aβ40 and A42 peptides. Our findings indicate that the β-sheet forming residues in the C-terminal region of the E22Δ mutant-type Aβ40 and Aβ42 peptides might serve as potential targets for the development of drugs which either destabilize β-sheet structure or stabilize helical structure for these residues to possibly inhibit the formation of toxic oligomeric species.

Previous studies have reported different trends in the effect of the E22Δ mutation on the toxicity as well as aggregation rates of the Aβ40 and Aβ42 peptides. In some cases, toxicity is reported to decrease for the Aβ42 peptide and increase for the Aβ40 peptide upon E22Δ mutation.[21,22] Other experimental measurements indicate that the E22Δ mutation does not increase the toxicity of either the Aβ40 or Aβ42 peptides but instead only inhibits synaptic function more than the wild-type Aβ alloforms.[14,23,24] Moreover, experimental measurements have reported conflicting trends for the impact of the E22Δ mutation on the aggregation rates of the Aβ peptide. While some studies report an increase in oligomerization but not fibrillization for the E22Δ mutant-type Aβ in comparison to the wild-type, other studies do report that the rate of fibrillization is increased upon E22Δ mutation.[14,22,23,25−27] Furthermore, some studies have reported that Aβ40 aggregates faster than Aβ42 upon E22Δ mutation, whereas other studies report an opposite trend.[22,23,25,26] Based on the structural and thermodynamic properties reported above, this study indicates that the aggregation rate of the Aβ40 peptide would increase upon E22Δ mutation but this effect would be much less prominent for the Aβ42 peptide upon E22Δ mutation. In addition, increased assembly rate is reported to be related to increased

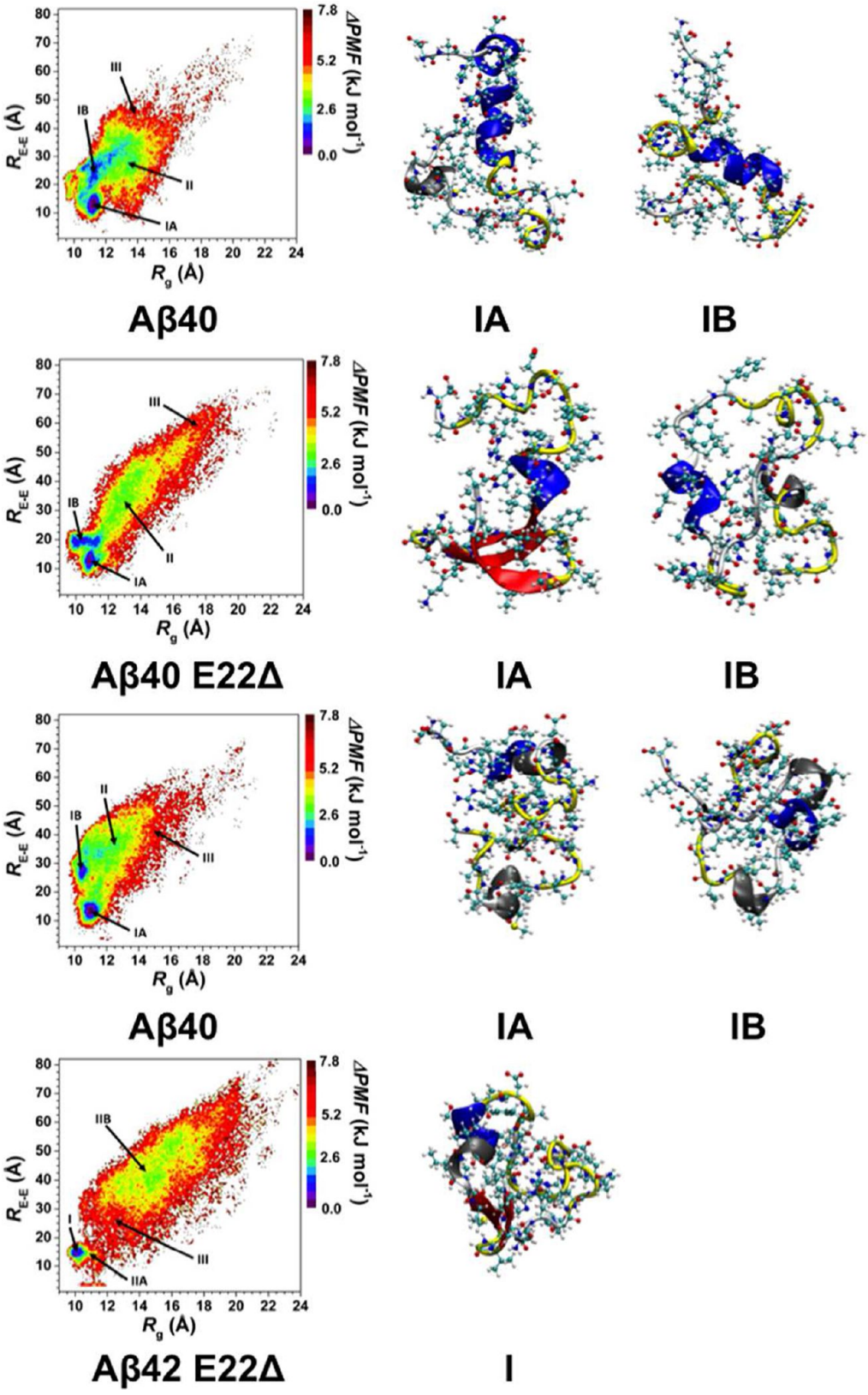

Figure 5. Change in the potential of mean force (ΔPMF) of the wild-type Aβ40 (Aβ40), E22Δ mutant-type Aβ40 (Aβ40 E22Δ), wild-type Aβ42 (Aβ42), and E22Δ mutant-type Aβ42 (Aβ42 E22Δ) peptides along the coordinates of radius of gyration (R_g) and end-to-end distance ($R_{E\text{-}E}$) in units of kJ mol^{-1}. Structures with representative tertiary and secondary structure characteristics of the most favorable PMF basins (basin IA and IB) for each of the wild- and E22Δ mutant-type Aβ peptides are displayed next to the PMF surface. The secondary structure components of each peptide structure are displayed by the color of the peptide backbone: α-helix (blue), 3_{10}-helix (gray), π-helix (purple), β-sheet (red), β-bridge (black), turn (yellow), and coil (white).

dx.doi.org/10.1021/cn300149j | ACS Chem. Neurosci. 2013, 4, 310−320

neurotoxicity for the wild-type Aβ40 and Aβ42 peptides.[20] Therefore, our results also indicate that the E22Δ Aβ40 peptide is more toxic than the wild-type Aβ40 and the E22Δ mutant-type Aβ42 peptide.

METHODS

All-atom replica exchange molecular dynamics (REMD) simulations[49] of the wild-type as well as E22Δ mutant-type Aβ40 and Aβ42 monomers in an aqueous solution environment were performed with the AMBER11 software package.[50] Following our recent studies, the initial structure of the wild-type Aβ42 monomer was taken from NMR measurements.[51] The E22Δ mutant-type Aβ42 initial structure was created by removing the Glu22 amino acid and connecting residues Ala21 and Asp23. Removing the last two residues (Ile41 and Ala42) from the wild- and E22Δ mutant-type Aβ42 resulted in the initial geometries of the wild- and E22Δ mutant-type Aβ40, respectively. The REMD simulations were performed utilizing the Amber ff99SB potential function[52] and Onufriev–Bashford–Case generalized Born implicit solvent model[53] for the protein and solution environment, respectively. As explained and demonstrated before,[40,54] an implicit solvent model was chosen to avoid configurational sampling limitations due to confined aqueous volume effects and inaccuracies in the specific heat of constant volume REMD simulations with explicit water reported by Parrinello and co-workers.[55] Langevin dynamics with a collision frequency of 2 ps^{-1} was used to control the temperature.[56] Particle mesh Ewald method was utilized to treat the long-range interactions with a cutoff value of 25 Å.[56,57] The temperatures of each replica for each peptide were exponentially distributed between 280 and 400 K, yielding exchange ratios of approximately 0.74 for all four Aβ peptides.[58] After energy minimization of the initial structures with the steepest descent method, the initial conformations of all peptides were equilibrated for 200 ps for each replica. Each system was then simulated using an integration time step of 2 fs for each replica, and trajectories were saved every 500 steps. Exchanges between replicas were attempted every 5 ps for each system. Each system was simulated for 100 ns for each replica (for each peptide) with a total simulation time of 2.4 μs.

The convergence of each REMD simulation was verified by calculating the time-dependent secondary structure abundances for all four Aβ peptides (see the Supporting Information). These results show that a simulation time of 60 ns is required to reach convergence. The structural and thermodynamic properties were then calculated for the structures of the wild-type and E22Δ mutant-type Aβ40 and Aβ42 peptides obtained after convergence from the replica closest to physiological temperature (310 K). The conformational Gibbs free energy (G) values of the simulated structures were approximated using the Molecular Mechanics/Generalized Born Surface Area method to assess the conformational preferences of each peptide.[59] The entropy was calculated using both the normal-mode analysis (NMA)[60] and the Schlitter methods[61,62] to assess the impact of harmonic and quasi-harmonic effects on the solute entropy. Following our previous work,[40] intramolecular peptide interactions occur when the centers of mass of two residues were within 9.0 Å from each other. In addition, an interaction is considered to be a salt bridge if a hydrogen bond exists between the two residues and the hydrogen bonded residues have opposite electrostatic charges.[40] For this study, if the distance between the donor and acceptor atoms of the hydrogen bond is ≤2.5 Å and the hydrogen bond angle is larger than 113°, then a hydrogen bond exists. To gain detailed insights into the secondary structure transitions of the Aβ peptides, we developed a new theoretical strategy. This new theoretical strategy is implemented in our recently developed ProtMet software. In this study, we used ProtMet to calculate the stability of secondary structure transitions between two different secondary structure components per residue in the conformations of the wild-type and E22Δ mutant-type Aβ proteins. See the Supporting Information for details. The convergence of the PMF and free energy values were validated following our recent studies.[40,54]

ASSOCIATED CONTENT

Supporting Information

Convergence figures for all four peptides and the description of our new theoretical strategy for calculating the residual secondary structure transition stabilities for intrinsically disordered proteins. Convergence figures for the secondary structure transition stabilities and the PMF surfaces of all four peptides. The probability distribution of the radius of gyration values for all four peptides. The secondary and tertiary structural properties of all four peptides along PMF surfaces. This material is available free of charge via the Internet at http://pubs.acs.org.

AUTHOR INFORMATION

Corresponding Author

*E-mail: orkid.coskuner@utsa.edu.

Author Contributions

T.K. and O.C. conceived and designed the simulations. O.W.-S. and T.K. performed the simulations. O.C. and O.W.-S. designed and coded the new theoretical strategy software. O.C., O.W.-S., and G.P. wrote the paper.

Funding

This research was supported by an allocation and computing resources provided by the National Science Foundation (Grant No. TG-CHE110044). The authors are thankful for the financial support from the University of Texas at San Antonio and Welch Foundation.

Notes

The authors declare no competing financial interest.

ACKNOWLEDGMENTS

The calculations and simulations were performed on Kraken at the National Institute for Computational Sciences and Texas Advanced Computing Center (TACC). The authors thank Michael G. Zagorski (CWRU), David Teplow (UCLA) and Hakan Ozoguz for the experimental data and for helpful discussions and support.

ABBREVIATIONS

APP, amyloid-β precursor protein; Aβ, amyloid-β; MTT, 3-(4,5-dimethylthiazo-2yl)-2,5-diphenyl tetrazolium bromide; LDH, lactate dehydrogenase; ThT, thioflavin T; REMD, replica exchange molecular dynamics; NMR, nuclear magnetic resonance; SDS, sodium dodecyl sulfate; NMA, normal-mode analysis

REFERENCES

(1) Reinhard, C., Hebert, S. S., and De Strooper, B. (2005) The amyloid-β precursor protein: integrating structure with biological function. *EMBO J. 24*, 3996–4006.

(2) Hardy, J., and Selkoe, D. J. (2002) Medicine - The amyloid hypothesis of Alzheimer's disease: Progress and problems on the road to therapeutics. *Science 297*, 353–356.

(3) Hardy, J. A., and Higgins, G. A. (1992) Alzheimer's disease: the amyloid cascade hypothesis. *Science 256*, 184–185.

(4) Hartmann, T., Bieger, S. C., Bruhl, B., Tienari, P. J., Ida, N., Allsop, D., Roberts, G. W., Masters, C. L., Dotti, C. G., Unsicker, K., and Beyreuther, K. (1997) Distinct sites of intracellular production for Alzheimer's disease Aβ 40/42 amyloid peptides. *Nat. Med. 3*, 1016–1020.

(5) Dahlgren, K. N., Manelli, A. M., Stine, W. B., Baker, L. K., Krafft, G. A., and LaDu, M. J. (2002) Oligomeric and fibrillar species of

amyloid-β peptides differentially affect neuronal viability. *J. Biol. Chem. 277*, 32046−32053.
(6) Selkoe, D. J. (1999) Translating cell biology into therapeutic advances in Alzheimer's disease. *Nature 399*, A23−A31.
(7) Younkin, S. G. (1995) Evidence That Aβ42 Is the Real Culprit in Alzheimers-Disease. *Ann. Neurol. 37*, 287−288.
(8) Krone, M. G., Baumketner, A., Bernstein, S. L., Wyttenbach, T., Lazo, N. D., Teplow, D. B., Bowers, M. T., and Shea, J. E. (2008) Effects of Familial Alzheimer's Disease Mutations on the Folding Nucleation of the Amyloid [beta]-Protein. *J. Mol. Biol. 381*, 221−228.
(9) Murakami, K., Irie, K., Morimoto, A., Ohigashi, H., Shindo, M., Nagao, M., Shimizu, T., and Shirasawa, T. (2003) Neurotoxicity and physicochemical properties of Aβ mutant peptides from cerebral amyloid angiopathy - Implication for the pathogenesis of cerebral amyloid angiopathy and Alzheimer's disease. *J. Biol. Chem. 278*, 46179−46187.
(10) Nilsberth, C., Westlind-Danielsson, A., Eckman, C. B., Condron, M. M., Axelman, K., Forsell, C., Stenh, C., Luthman, J., Teplow, D. B., Younkin, S. G., Naslund, J., and Lannfelt, L. (2001) The 'Arctic' APP mutation (E693G) causes Alzheimer's disease by enhanced Aβ protofibril formation. *Nat. Neurosci. 4*, 887−893.
(11) Grabowski, T. J., Cho, H. S., Vonsattel, J. P. G., Rebeck, G. W., and Greenberg, S. M. (2001) Novel amyloid precursor protein mutation in an Iowa family with dementia and severe cerebral amyloid angiopathy. *Ann. Neurol. 49*, 697−705.
(12) Wakutani, Y., Watanabe, K., Adachi, Y., Wada-Isoe, K., Urakami, K., Ninomiya, H., Saido, T. C., Hashimoto, T., Iwatsubo, T., and Nakashima, K. (2004) Novel amyloid precursor protein gene missense mutation (D678N) in probable familial Alzheimer's disease. *J. Neurol., Neurosurg. Psychiatry 75*, 1039−1042.
(13) Janssen, J. C., Beck, J. A., Campbell, T. A., Dickinson, A., Fox, N. C., Harvey, R. J., Houlden, H., Rossor, M. N., and Collinge, J. (2003) Early onset familial Alzheimer's disease - Mutation frequency in 31 families. *Neurology 60*, 235−239.
(14) Tomiyama, T., Nagata, T., Shimada, H., Teraoka, R., Fukushima, A., Kanemitsu, H., Takuma, H., Kuwano, R., Imagawa, M., and Ataka, S. (2008) A new amyloid-β variant favoring oligomerization in Alzheimer's-type dementia. *Ann. Neurol. 63*, 377−387.
(15) Yang, M. F., and Teplow, D. B. (2008) Amyloid β-Protein Monomer Folding: Free-Energy Surfaces Reveal Alloform-Specific Differences. *J. Mol. Biol. 384*, 450−464.
(16) Luttmann, E., and Fels, G. (2006) All-atom molecular dynamics studies of the full-length β-amyloid peptides. *Chem. Phys. 323*, 138−147.
(17) Sgourakis, N. G., Yan, Y. L., McCallum, S. A., Wang, C. Y., and Garcia, A. E. (2007) The Alzheimer's peptides Aβ 40 and 42 adopt distinct conformations in water: A combined MD/NMR study. *J. Mol. Biol. 368*, 1448−1457.
(18) Lim, K. H., Collver, H. H., Le, Y. T. H., Nagchowdhuri, P., and Kenney, J. M. (2007) Characterizations of distinct amyloidogenic conformations of the Aβ(1−40) and (1−42) peptides. *Biochem. Biophys. Res. Commun. 353*, 443−449.
(19) Hou, L. M., Shao, H. Y., Zhang, Y. B., Li, H., Menon, N. K., Neuhaus, E. B., Brewer, J. M., Byeon, I. J. L., Ray, D. G., Vitek, M. P., Iwashita, T., Makula, R. A., Przybyla, A. B., and Zagorski, M. G. (2004) Solution NMR studies of the Aβ(1−40) and Aβ(1−42) peptides establish that the met35 oxidation state affects the mechanism of amyloid formation. *J. Am. Chem. Soc. 126*, 1992−2005.
(20) Roychaudhuri, R., Yang, M., Hoshi, M. M., and Teplow, D. B. (2009) Amyloid beta-Protein Assembly and Alzheimer Disease. *J. Biol. Chem. 284*, 4749−4753.
(21) Takuma, H., Teraoka, R., Mori, H., and Tomiyama, T. (2008) Amyloid-β E22Δ variant induces synaptic alteration in mouse hippocampal slices. *NeuroReport 19*, 615.
(22) Ovchinnikova, O. Y., Finder, V. H., Vodopivec, I., Nitsch, R. M., and Glockshuber, R. (2011) The Osaka FAD Mutation E22Δ Leads to Formation of a Previously Unknown Type of Amyloid β Fibrils and Modulates Aβ Neurotoxicity Fibrillization and Neurotoxicity of E22Δ Variants of Aβ. *J. Mol. Biol. 408*, 780−791.
(23) Suzuki, T., Murakami, K., Izuo, N., Kume, T., Akaike, A., Nagata, T., Nishizaki, T., Tomiyama, T., Takuma, H., and Mori, H. (2010) E22Δ Mutation in Amyloid β-Protein Promotes β-Sheet Transformation, Radical Production, and Synaptotoxicity, But Not Neurotoxicity. *Int. J. Alzheimer's Dis. 2011*, 1−8.
(24) Tomiyama, T., Matsuyama, S., Iso, H., Umeda, T., Takuma, H., Ohnishi, K., Ishibashi, K., Teraoka, R., Sakama, N., and Yamashita, T. (2010) A mouse model of amyloid-β oligomers: their contribution to synaptic alteration, abnormal tau phosphorylation, glial activation, and neuronal loss in vivo. *J. Neurosci. 30*, 4845−4856.
(25) Inayathullah, M., and Teplow, D. B. (2011) Structural dynamics of the ΔE22 (Osaka) familial Alzheimer's disease-linked amyloid β-protein. *Amyloid*, 1−12.
(26) Poduslo, J. F., Howell, K. G., Olson, N. C., Ramirez-Alvarado, M., and Kandimalla, K. K. (2012) Alzheimer's Disease Amyloid β-Protein Mutations and Deletions That Define Neuronal Binding/Internalization As Early Stage Nonfibrillar/Fibrillar Aggregates and Late Stage Fibrils. *Biochemistry 51*, 3993−4003.
(27) Cloe, A. L., Orgel, J. P. R. O., Sachleben, J. R., Tycko, R., and Meredith, S. C. (2011) The Japanese Mutant Aβ (ΔE22-Aβ(1−39)) Forms Fibrils Instantaneously, with Low-Thioflavin T Fluorescence: Seeding of Wild-Type Aβ(1−40) into Atypical Fibrils by ΔE22-Aβ(1−39). *Biochemistry 50*, 2026−2039.
(28) Fawver, J. N., Duong, K. T., Wise-Scira, O., Schall, H. E., Coskuner, O., Zhu, X., Colom, L. V., and Murray, I. V. J. (2012) Probing and Trapping a Sensitive Conformation: Amyloid-β Fibrils, Oligomers, and Dimers. *J. Alzheimer's Dis. 32*, 197−215.
(29) Simmons, L. K., May, P. C., Tomaselli, K. J., Rydel, R. E., Fuson, K. S., Brigham, E. F., Wright, S., Lieberburg, I., Becker, G. W., and Brems, D. N. (1994) Secondary structure of amyloid-β peptide correlates with neurotoxic activity in vitro. *Mol. Pharmacol. 45*, 373−379.
(30) Teplow, D. B. (1998) Structural and kinetic features of amyloid β-protein fibrillogenesis. *Amyloid\ 5*, 121−142.
(31) Pike, C. J., Walencewiczwasserman, A. J., Kosmoski, J., Cribbs, D. H., Glabe, C. G., and Cotman, C. W. (1995) Structure-Activity Analyses of β-Amyloid Peptides - Contributions of the β25−35 Region to Aggregation and Neurotoxicity. *J. Neurochem. 64*, 253−265.
(32) Kabsch, W., and Sander, C. (1983) Dictionary of Protein Secondary Structure - Pattern-Recognition of Hydrogen-Bonded and Geometrical Features. *Biopolymers 22*, 2577−2637.
(33) Lazo, N. D., Grant, M. A., Condron, M. C., Rigby, A. C., and Teplow, D. B. (2005) On the nucleation of amyloid β-protein monomer folding. *Protein Sci. 14*, 1581−1596.
(34) Borreguero, J. M., Urbanc, B., Lazo, N. D., Buldyrev, S. V., Teplow, D. B., and Stanley, H. E. (2005) Folding events in the 21−30 region of amyloid-β-protein (Aβ) studied in silico. *Proc. Natl. Acad. Sci. U.S.A. 102*, 6015−6020.
(35) Cruz, L., Urbanc, B., Borreguero, J. M., Lazo, N. D., Teplow, D. B., and Stanley, H. E. (2005) Solvent and mutation effects on the nucleation of amyloid β-protein folding. *Proc. Natl. Acad. Sci. U.S.A. 102*, 18258−18263.
(36) Baumketner, A., Bernstein, S. L., Wyttenbach, T., Lazo, N. D., Teplow, D. B., Bowers, M. T., and Shea, J. E. (2006) Structure of the 21−30 fragment of amyloid β-protein. *Protein Sci. 15*, 1239−1247.
(37) Baumketner, A., Bernstein, S. L., Wyttenbach, T., Bitan, G., Teplow, D. B., Bowers, M. T., and Shea, J. E. (2006) Amyloid β-protein monomer structure: A computational and experimental study. *Protein Sci. 15*, 420−428.
(38) Tarus, B., Straub, J. E., and Thirumalai, D. (2006) Dynamics of Asp23-Lys28 salt-bridge formation in Aβ(10−35) monomers. *J. Am. Chem. Soc. 128*, 16159−16168.
(39) Reddy, G., Straub, J. E., and Thirumalai, D. (2009) Influence of Preformed Asp23-Lys28 Salt Bridge on the Conformational Fluctuations of Monomers and Dimers of A beta Peptides with Implications for Rates of Fibril Formation. *J. Phys. Chem B. 113*, 1162−1172.

(40) Wise-Scira, O., Xu, L., Kitahara, T., Perry, G., and Coskuner, O. (2011) Amyloid-β peptide structure in aqueous solution varies with fragment size. *J. Chem. Phys. 135*, 205101.
(41) Sgourakis, N. G., Merced-Serrano, M., Boutsidis, C., Drineas, P., Du, Z. M., Wang, C. Y., and Garcia, A. E. (2011) Atomic-Level Characterization of the Ensemble of the Aβ(1−42) Monomer in Water Using Unbiased Molecular Dynamics Simulations and Spectral Algorithms. *J. Mol. Biol. 405*, 570−583.
(42) Sticht, H., Bayer, P., Willbold, D., Dames, S., Hilbich, C., Beyreuther, K., Frank, R. W., and Rosch, P. (1995) Structure of Amyloid Aβ(1−40)-Peptide of Alzheimers-Disease. *Eur. J. Biochem. 233*, 293−298.
(43) Triguero, L., Singh, R., and Prabhakar, R. (2008) Comparative Molecular Dynamics Studies of Wild-Type and Oxidized Forms of Full-Length Alzheimer Amyloid β-Peptides Aβ(1−40) and Aβ(1−42). *J. Phys. Chem. B 112*, 7123−7131.
(44) Jarrett, J. T., Berger, E. P., and Lansbury, P. T. (1993) The Carboxy Terminus of the β-Amyloid Protein Is Critical for the Seeding of Amyloid Formation - Implications for the Pathogenesis of Alzheimers-Disease. *Biochemistry 32*, 4693−4697.
(45) Lomakin, A., Chung, D. S., Benedek, G. B., Kirschner, D. A., and Teplow, D. B. (1996) On the nucleation and growth of amyloid β-protein fibrils: Detection of nuclei and quantitation of rate constants. *Proc. Natl. Acad. Sci. U.S.A. 93*, 1125−1129.
(46) Lomakin, A., Teplow, D. B., Kirschner, D. A., and Benedek, G. B. (1997) Kinetic theory of fibrillogenesis of amyloid β-protein. *Proc. Natl. Acad. Sci. U.S.A. 94*, 7942−7947.
(47) Bitan, G., Kirkitadze, M. D., Lomakin, A., Vollers, S. S., Benedek, G. B., and Teplow, D. B. (2003) Amyloid β-protein (Aβ) assembly: Aβ40 and Aβ42 oligomerize through distinct pathways. *Proc. Natl. Acad. Sci. U.S.A. 100*, 330−335.
(48) Walsh, D. M., Lomakin, A., Benedek, G. B., Condron, M. M., and Teplow, D. B. (1997) Amyloid β-protein fibrillogenesis - Detection of a protofibrillar intermediate. *J. Biol. Chem. 272*, 22364−22372.
(49) Sugita, Y., and Okamoto, Y. (1999) Replica-exchange molecular dynamics method for protein folding. *Chem. Phys. Lett. 314*, 141−151.
(50) Case, D., Darden, T., Cheatham, T., Simmerling, C., Wang, J., Duke, R., Luo, R., Walker, R., Zhang, W., and Merz, K. (2010) *AMBER 11*, University of California, San Francisco.
(51) Tomaselli, S., Esposito, V., Vangone, P., van Nuland, N. A. J., Bonvin, A. M. J. J., Guerrini, R., Tancredi, T., Temussi, P. A., and Picone, D. (2006) The α-to-β Conformational Transition of Alzheimer's Aβ-(1−42) Peptide in Aqueous Media is Reversible: A Step by Step Conformational Analysis Suggests the Location of β Conformation Seeding. *ChemBioChem 7*, 257−267.
(52) Simmerling, C., Hornak, V., Abel, R., Okur, A., Strockbine, B., and Roitberg, A. (2006) Comparison of multiple amber force fields and development of improved protein backbone parameters. *Proteins 65*, 712−725.
(53) Case, D. A., Onufriev, A., and Bashford, D. (2004) Exploring protein native states and large-scale conformational changes with a modified generalized born model. *Proteins 55*, 383−394.
(54) Wise-Scira, O., Xu, L., Perry, G., and Coskuner, O. (2012) Structures and free energy landscapes of aqueous zinc(II)-bound amyloid-β(1−40) and zinc(II)-bound amyloid-β(1−42) with dynamics. *J. Biol. Inorg. Chem. 17*, 927−938.
(55) Prakash, M. K., Barducci, A., and Parrinello, M. (2011) Replica Temperatures for Uniform Exchange and Efficient Roundtrip Times in Explicit Solvent Parallel Tempering Simulations. *J. Chem. Theory Comput. 7*, 2025−2027.
(56) Allen, M. P., and Tildesley, D. J. (1999) *Computer simulation of liquids*, Clarendon Press: Oxford.
(57) Frenkel, D., and Smit, B. (2002) *Understanding molecular simulation: from algorithms to applications*, Vol. *1*, Academic Press: San Diego.
(58) van der Spoel, D., and Patriksson, A. (2008) A temperature predictor for parallel tempering simulations. *Phys. Chem. Chem. Phys. 10*, 2073−2077.
(59) Kollman, P. A., Massova, I., Reyes, C., Kuhn, B., Huo, S. H., Chong, L., Lee, M., Lee, T., Duan, Y., Wang, W., Donini, O., Cieplak, P., Srinivasan, J., Case, D. A., and Cheatham, T. E. (2000) Calculating structures and free energies of complex molecules: Combining molecular mechanics and continuum models. *Acc. Chem. Res. 33*, 889−897.
(60) Case, D. A. (1994) Normal-Mode Analysis of Protein Dynamics. *Curr. Opin. Struct. Biol. 4*, 285−290.
(61) Schlitter, J. (1993) Estimation of Absolute and Relative Entropies of Macromolecules Using the Covariance-Matrix. *Chem. Phys. Lett. 215*, 617−621.
(62) Schlitter, J., Swegat, W., Kruger, P., and Wollmer, A. (2003) MD simulation of protein-ligand interaction: Formation and dissociation of an insulin-phenol complex. *Biophys. J. 84*, 1493−1506.